Development of a novel type activated carbon fiber filter for indoor air purification

Development of a novel type activated carbon fiber filter for indoor air purification

Jelle Roegiers [†], *Siegfried Denys*[†,*]

† Sustainable Energy, Air & Water Technology, Department of Bioscience Engineering, University of Antwerp, Groenenborgerlaan 171, B-2020 Antwerp, Belgium.

* E-mail: Siegfried.Denys@uantwerp.be

Fax: +32 3 265 32 25. Tel: +32 3 265 32 30.

Keywords

Computational Fluid Dynamics; Activated Carbon Fiber; thermo-electrical regeneration; VOC adsorption; Filter design

Highlights

- Activated carbon fiber filter with pleated structure
- Equipotential conductors in the pleat-tips for thermo-electrical regeneration
- Adsorption, pressure drop and electrical properties were determined
- Optimization of the filter configuration with CFD

*Corresponding author. E-mail: Siegfried.Denys@uantwerp.be

1. Abstract

A novel type of activated carbon fiber filter was developed for indoor air purification. The filter is equipped with electrodes for thermo-electrical regeneration at the point of saturation. The electrodes are arranged in such a way that the filter forms a pleated structure with an electrode in the tip of each pleat. This allows for a uniform temperature distribution on the filter surface during the regeneration process and the pleated structure reduces the overall pressure drop across the filter. The latter was validated by Computational Fluid Dynamics, using Darcy-Forchheimer parameters derived in previous work. The CFD model was further used to perform a virtual sensitivity study in search for the optimal ACF filter design by varying the pleat length, pleat height and filter thickness. Finally, adsorption and desorption properties were investigated with acetaldehyde and toluene as model compounds. Freundlich and Langmuir adsorption parameters, derived in previous work were successfully validated with a Multiphysics model.

2. Introduction

During the last decades, increasing attention has been paid to the presence and influence of indoor volatile organic compounds (VOCs) [1–7]. Even at ppb-level concentrations these pollutants can be detrimental for both human health and environment. To oppose these health and environmental risks, VOCs need to be eliminated from the indoor air. In a previous work, we investigated activated carbon fibers for adsorption of indoor air pollutants [8]. ACF filters are especially interesting because of their high adsorption capacity and fast kinetics [9]. Moreover, it was observed that the filter exhibits a limited pressure drop, even at high air flow rates. The latter is an important criterion if the filter device should be retrofitted in an HVAC system, since the fan is specially tailored to the pressure losses occurring in the vent duct.

Incorporating a low permeable filtering device would negatively influence the fresh air delivery rate of the system or would require a more powerful fan along with higher energy demand. Based on the Darcy-Forchheimer parameters, determined in previous work, and in combination with Computational Fluid Dynamics (CFD), we were able to develop a filter device with a low pressure drop at realistic HVAC flow rates while maintaining a high filter surface area. The basic principle of the concept was the use of pleats instead of a planar filter. Pleated filters have the advantage that pressure loss can be lowered by increasing the filter surface area, which is commonly applied to HEPA filters [10–14]. Although the air flow is initially accelerated in the pleats, when passing through the filter medium, the flow can be drastically decreased due to the widening of the cross-sectional area. The latter is responsible for the low pressure drop in accordance with Darcy's Law. In addition, the pleated filter device is inventively engineered in such a way that is also capable of thermo-electrical regeneration, which makes it unique. Another major advantage is that such a filter system can easily be combined with other air purification technologies, in which the pollutants are first concentrated on the filter cloth and subsequently released, i.e. thermo-electrically regenerated, and mineralized in short period of time (by drastically reducing mass transfer limitations). A lab-scale prototype was constructed to perform VOC adsorption/desorption experiments. Since adsorption of acetaldehyde was successfully modelled in previous work, based on Langmuir and Freundlich isotherms, the adsorption experiments could serve as a validation test for the Multiphysics model. Activated carbon filters in general are known for their affinity towards apolar compounds over polar compounds, such as acetaldehyde. Therefore, additional adsorption experiments were performed with toluene in order to compare the filters affinity for polar and apolar VOCs. The affinity of the ACF filter towards apolar compounds is not only reflected by the adsorption isotherm, but also by the required desorption temperature for complete regeneration [15–19]. Desorbing apolar VOCs usually requires high temperatures,

due to a strong bond with the filter surface, while lower temperatures are sufficient in the case of polar VOCs [20–22]. This work aims to study the feasibility of a novel type ACF filter system for indoor air purification of VOCs in terms of the pressure loss, adsorption capacity and energy consumption during desorption, with the aid of Computational Fluid Dynamics.

3. Methodology

3.1 ACF filter concept

Filtering systems are often faced with an inevitable trade-off between adsorption capacity and pressure drop across the filter medium, as is the case with the frequently used Granular activated carbon (GAC) packed bed. One of the main advantages of ACF is that it has a great flexibility in the form of a woven cloth or felt [23]. Therewith, a great opportunity rises to engineer an ACF filter system that tackles this trade-off problem. The idea for a novel ACF filter was initially founded on the concept of pleated dust filters, which are widely used in HVAC systems and vacuum cleaners to filter particulate matter [10–14]. Limited but promising research has been dedicated to pleated ACF filters, predominantly in the form of cylindrical pleated filtering devices [9,10,24,25]. However, none of these systems feature the ability to thermo-electrically regenerate, which is another main advantage of ACF filters. For the new concept, we proposed a rectangular pleated filter device with narrow conductors in the tips of the pleats (Figure 1). Consequently, the conductors on each side of the pleated filter were connected to a single central conductor, which in turn was coupled to an electrical DC power source (Delta Elektronika, 0-35V/0-45A). This was repeated for the conductors on the other side of the pleated filter. Thus, when a voltage is applied over the ACF filter, the electrical current is uniformly distributed to all elements in the pleated filter, similar to an electrical circuit with parallel resistances. The adsorbent material used for the filter system is the commercially available ACF cloth FM10 (Calgon Corp.) which has been well studied in

the past on its adsorption capacity for VOCs [16,26,27]. In this work, an element is defined as the substantially rectangular part of ACF sheet between two conductors and one pleat has two elements, which are each part of two adjacent pleats, each having a conductor at its tip.

According to Ohm's law, the electrical current flowing through the entire ACF filter can be calculated as:

$$I = \frac{V}{R_{par}};\ R_{par} = \left(\sum_{i}^{n} \frac{1}{R_{element,i}} \right)^{-1} \quad \textbf{1}$$

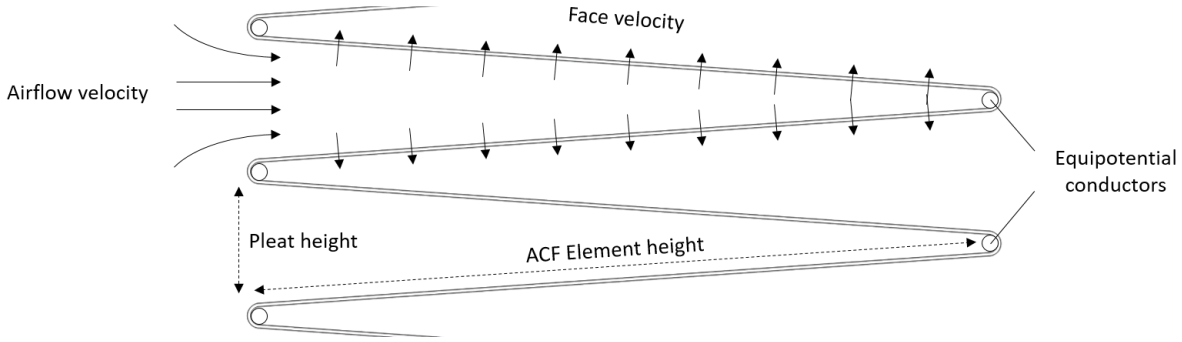

Figure 1 Pleated ACF filter with electrical conductors in the tip of each pleat to induce the Joule-effect

With R_{par} the parallel electrical resistance (Ω), $R_{element,i}$ the electrical resistance of an individual element of the ACF (Ω), i.e. one planar ACF sheet between two conductors, and n the total number of ACF sheets in the filter device. Based on the assumption that the electrical current is uniformly distributed and that the resistance of each ACF pleat is identical, we could hypothesize that:

$$R_{par} = \frac{R_{element,i}}{n} \quad \textbf{2}$$

Furthermore, the electrical resistance can be described as:

$$R_{element,i} = \frac{\rho_e}{t}\frac{l}{w} \quad \textbf{3}$$

Wherein, ρ_e represents the electrical resistivity (Ωm), l the length of the ACF element (m), i.e. the distance from conductor to conductor, t the filter thickness and w the width of the ACF element that is in direct contact with the conductor. The electrical resistivity is in turn a temperature dependent property, often described as [9]:

$$\frac{\rho_e}{\rho_0} = \exp\left[\alpha_0\left(\frac{1}{T} - \frac{1}{T_0}\right)\right] \quad \textbf{4}$$

With ρ_0 the electrical resistivity (Ωm) at temperature T_0 (K), T the average temperature of the ACF filter (K) and α_0 the thermal coefficient at temperature T_0 (K). In summary, if we could determine the value of ρ_0 and α_0, it is possible to derive the total resistance of the ACF filter R_{par} and hence, the required electrical power to heat the ACF filter to a certain temperature for regeneration purposes. The values of ρ_0 and α_0 were determined by measuring the surface temperature of the ACF filter with a thermocouple (TC Direct, Type K), in setups with different pleat sizes and by alternating the voltage (0-32V). Thereto, a lab-scale prototype of

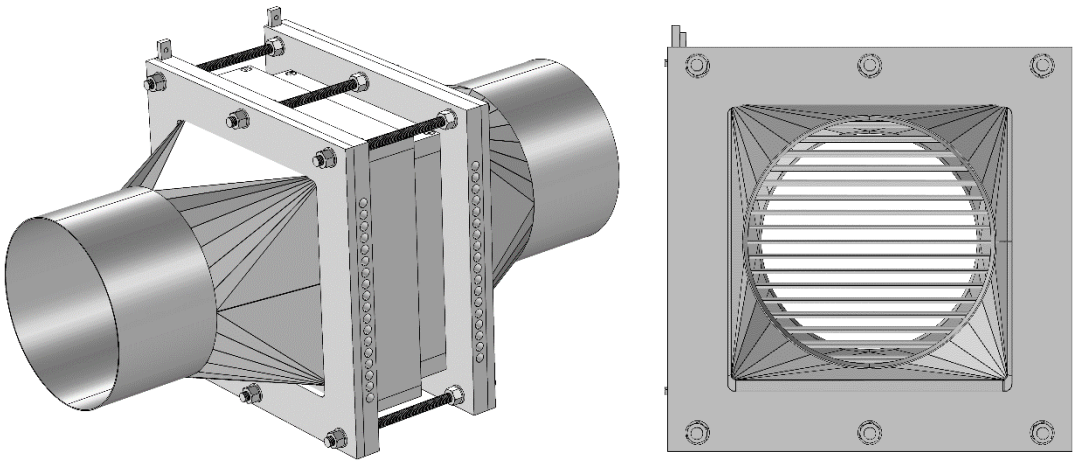

Figure 2 ACF filter prototype with built-in thermo-electrical regeneration system

the filter was constructed (Figure 2).

The airflow enters the device through a 160mm diameter duct, which then expands to a rectangular compartment (185mm x 185mm) that contains the FM10 ACF filter and at the end it is reduced back to a 160mm diameter outlet duct. The rectangular compartment contains 18 steel conductors (7mm^2) on both sides and on each side connected to a central copper conductor. The two central copper conductors are coupled to the DC power source to supply a voltage. The ACF filter is stretched over the conductors and fixated at the both ends. A system with threaded rods and nuts made it possible to alter the distance between the two sides of conductors, i.e. elongating the device in the direction of the air flow. This way, the ACF filter could be stretched out to a maximum, by tightening the nuts, forming perfectly shaped pleats and assure good contact with the conductors.

3.2 Pressure curves validation

In previous work, the Darcy-Forchheimer parameters of the FM10 ACF-filter were determined based on experiments where the air flowed perpendicular to the surface area of the ACF filter and confirmed by CFD simulations [8]. Since the current prototype contains a pleated filter, pressure drop is not only generated by the filter medium, but also by viscous drag in the pleat spacings. In order to verify if the CFD model could simulate the flow in pleated ACF filters, the pressure drop across different pleat dimensions in the device was studied in a closed circuit vent duct with an inline duct fan, similar as in previous work [8]. The different setups that were investigated for pressure drop are listed in Tabel 1 and pressure drop measurements were repeated in 3-fold for each setup. In setup 1, the filter does not contain pleats, but instead is a simple planar surface. The velocity was measured in a 100mm diameter vent duct of the closed circuit setup by a hotwire air velocity sensor (CTV 110,

KIMO instruments). The listed setups were also used to determine the parameters ρ_0 and α_0, as described above.

Tabel 1 Setup specifications

	Setup1	**Setup2**	**Setup3**
Number of pleats	none	7 pleats	14 pleats
Number of conductors	0	7	14
Number of elements	0	8	15
Element Height (mm)	/	111	112
Element width (mm)	/	185	185
Surface area (m²)	0.034	0.164	0.311
Adsorbent mass (g)	4.454	21.484	40.741

The air stream was simulated as an incompressible flow with the 'Free and Porous Media Flow' physics interface in COMSOL 5.5. The filter was defined as a porous medium with permeability κ=2.71×10^{-10} m² and Forchheimer drag β=64798 m^{-1}, as determined in previous work [8]. The solution for the pressure drop was extracted by simultaneously solving the mass continuity equation, the governing equations for the free flow (k-ε-turbulent model) and the equations for flow in porous media:

$$\rho\nabla(\mathbf{u}) = 0$$

$$\rho(\mathbf{u}\cdot\nabla)\mathbf{u} = \nabla\cdot\left(-p\mathbf{I} + (\mu+\mu_T)(\nabla\mathbf{u} + (\nabla\mathbf{u})^T)\right) \quad 6$$

$$\frac{\rho}{\epsilon_p}\left((\mathbf{u}\cdot\nabla)\frac{\mathbf{u}}{\epsilon_p}\right) = \nabla\cdot\left(-p\mathbf{I} + \frac{\mu}{\epsilon_p}(\nabla\mathbf{u} + (\nabla\mathbf{u})^T) - \frac{2\mu}{3\epsilon_p}(\nabla\cdot\mathbf{u})I\right) - (\mu\kappa^{-1} + \beta|\mathbf{u}|)\mathbf{u} \quad 7$$

Wherein ρ represents the air density (1.2041 kg/m³), **u** the velocity vector (m/s), **I** the identity matrix, p the pressure (Pa), μ the dynamic viscosity (Pa·s) and μ_T the eddy viscosity (Pa·s), derived by the k-ε turbulence model. A parametric sweep of velocity inputs ranging from 0 to 4.5 m/s with 0.1 m/s intervals was performed in order to obtain a smooth pressure-velocity curve in the same range as the experimental pressure-velocity curves.

3.3 ACF filter development

A validated CFD model is a very useful tool for development and upscale purposes. As a demonstration of the capabilities of CFD modelling, a virtual sensitivity study has been performed in search for the optimal ACF filter design. The base configuration is a 0.6m x 0.6m cross-section module with a variable length, pleat height and filter thickness and is representative for commercially available GAC units for indoor air applications [28]. The goal was to optimize the filter design with respect to pressure drop and adsorption capacity. The length of the module, i.e. in the direction of the airflow, was altered between 0.3 and 0.6m, the filter cloth thickness between 0.5, 1 and 1.5mm, and the pleat height between 2.76mm and 3.90mm. Each configuration contains a maximum number of pleats (so the elements are stacked horizontally), but the number of pleats differ due to variations in filter thickness and conductor diameter. The height of the pleat corresponds to typical conductor dimensions of 6mm² and 12mm² respectively. A typical HVAC flow rate of 2.5 m/s was imposed as a boundary condition in all cases [28].

3.4 Adsorption/Desorption

In previous work, the FM10 ACF filter has already been investigated with regard to adsorption capacity of acetaldehyde and an adsorption isotherm was constructed at 20°C [8]. In this paper, adsorption of acetaldehyde was further studied for the pleated prototype (Setup2) as a validation method. The study was performed in an airtight climate chamber (1.2m³) with two fixed fans on the ceiling to ensure homogeneous mixture of the air inside. The prototype was placed in the center of the chamber and fitted with a fan (Wallair W-style, 290 m³/h). At the start of the experiment, a liquid volume acetaldehyde was injected by a capillary piston pipet (Microman E M100E) and immediately evaporated. The concentration inside the climate chamber was measured online by a Compact GC-FID 4.0 analyzer (Interscience). When the concentration reached a steady-state, the acetaldehyde in the air was in equilibrium with the concentration adsorbed on the ACF filter. Hence, the adsorbed amount of acetaldehyde could be derived from the injected volume and the equilibrium concentration. The same protocol was repeated, each time with an increased sample volume with a prospect to eventually construct an isotherm at 20°C. Subsequently, the obtained isotherm was compared with the Langmuir and Freundlich isotherms, which were constructed in previous work, described by the following equations:

$$c_{ads} = c_{ads,max} \frac{K_{Langm} c}{1 + K_{Langm} c} \quad \textbf{8}$$

$$c_{ads} = K_{Freund.} c^{1/n} \quad \textbf{9}$$

Since activated carbon tends to have a higher affinity towards more apolar VOCs, additional experiments were conducted with toluene. In the same way, the isotherm for toluene at 20°C was constructed and compared to the isotherm of acetaldehyde, i.e. a polar compound. Besides adsorption capacity, the ACF filters affinity for apolar compounds is usually reflected in the required desorption temperature for complete regeneration. The regeneration efficiency was investigated in terms of temperature and electrical power. For the experiment, setup 2

(Tabel 1) was placed in the climate chamber and a liquid volume of either acetaldehyde or toluene was injected. Subsequently, the fan was powered and adsorption occurred until equilibrium was reached. The excess concentration of acetaldehyde (or toluene) in air was vented out of the climate chamber during a 30 min period, which should be a sufficient amount of time according to Ryu et al. (2000) and Xie et al. (2016) [29,30]. During the purging process, a voltage between 0 and 32V was applied to heat the filter to a certain temperature based on the Joule-effect. Due to an increase in temperature, the VOC is desorbed to a certain extend and vented out. After 30 min, the climate chamber was sealed again and an equal liquid volume of VOC was yet again injected. Based on the new equilibrium concentration that was established, the fraction of VOC that remained on the filter after desorption could be established and therewith the regeneration efficiency could be derived. This protocol was repeated with different applied voltages and thus different desorption temperatures. This method allowed to determine and compare the regeneration efficiency in function of the filter temperature for both acetaldehyde (polar) and toluene (apolar).

4. Results and discussion

4.1 Pressure curves

Experimental pressure-velocity curves were constructed based on pressure drop measurements in the closed-circuit vent duct (Figure 3). The measurements were performed in triplicate and the standard deviation of the results is represented by error-bars in the graph. Airflow through the planar filter surface resulted in a steep pressure-velocity curve, as expected. Since the Darcy-Forchheimer parameters were derived in a similar (yet smaller) setup, a good agreement was expected between experimental data and the CFD simulation results. This was indeed the case as reflected by a coefficient of determination R^2=0.997. In the case of a pleated filter, as for setup 2, a drastic reduction in pressure drop was observed.

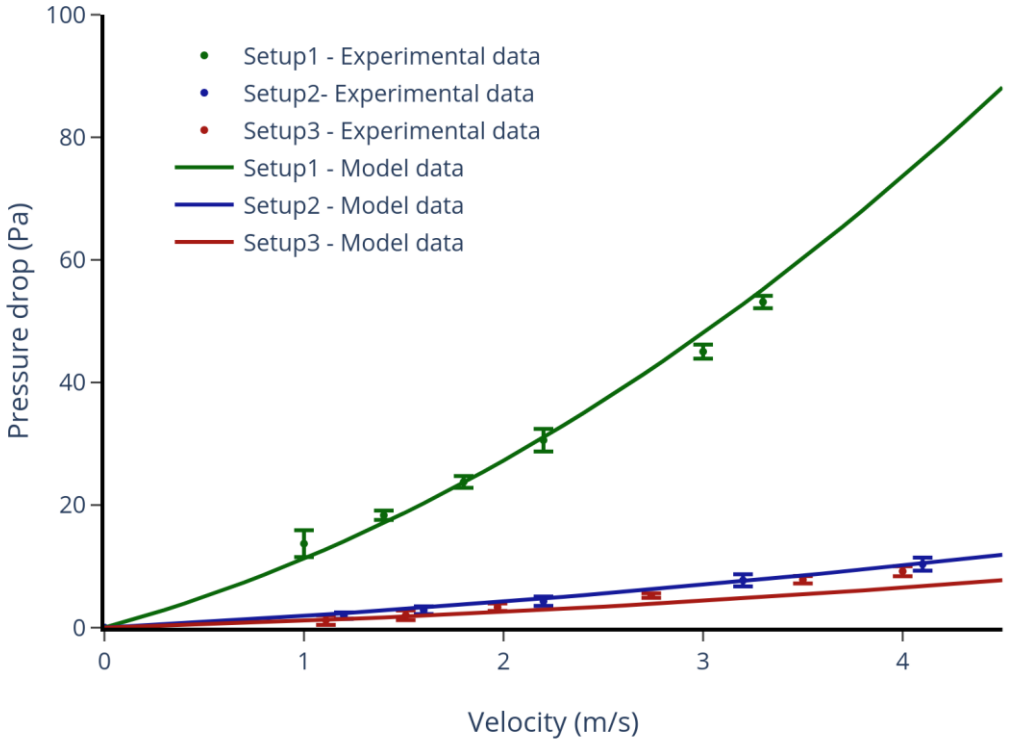

Figure 3 Experimental pressure-velocity curves for the different setups and the respective CFD model fit.

Due to the increase in cross-sectional filter section, the air flow velocity is reduced and hence, the pressure drop in accordance with Darcy's law. The pleat height is relatively high, which makes the influence of viscous drag negligible. The same trend was noticed in setup 3. However, the pressure-velocity curves of setup 2 and 3 are in close proximity to each other, suggesting that viscous effects have an impact on the total pressure drop in setup 3. These different cases stress out the importance of gaining insights regarding the trade-off between viscous drag and porous medium pressure drop, especially in terms of pleat height or filter development in general. Therefore, a CFD model that is able to predict these phenomena is of great value. The simulated pressure drops for the respective pleated setups are shown in Figure 3 with a coefficient of determination of 0.993 and 0.535 for setup 2 and 3 respectively. The model was capable of predicting the lower pressure drop due to a decrease in face velocity through the filter. As an example, a velocity of 1 m/s in the 100mm diameter vent duct of the closed circuit setup, results in a 0.230 m/s facial velocity in the 0.185m x 0.185m cross-sectional area of setup 1. The same air flow rate results in a facial velocity of only 0.052

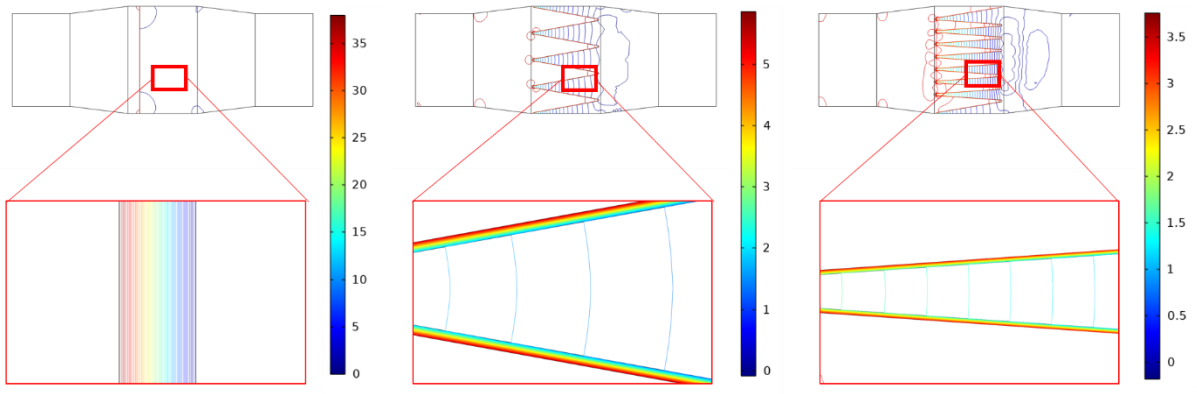

Figure 4 Pressure contours (50) of setup 1 to 3 (from right to left) for an inflow velocity of 2.5 m/s.

m/s in Setup 2, due to a much higher filter surface. In setup 3 the facial velocity averages 0.028 m/s, causing an ever lower pressure drop over the filter. From these results, we can conclude that the CFD model can accurately simulate the pressure drop in pleated ACF filters.

The effect of viscous drag was also represented in Figure 4, where 50 pressure contours are shown for the different setups, for an inflow velocity of 2.5 m/s. The pressure drop in setup 1 is exclusively due to the air flow through the filter and solely depends on the filter thickness at a specific air flow velocity. The pressure drop over the filter is still major contributor in the case of setup 2 and 3, but notice the presence of pressure contours between the pleats, which can be attributed to viscous drag. As the pleat height decreases, the pressure drop due to viscous drag increases, as can be seen by the increased number of pressure contours in setup 3 compared to setup 2. Based on these conclusions, we can be confident to use the CFD model to perform a sensitivity analysis of the pressure drop with respect to filter thickness (0.5,1 and 1.5mm), pleat height (2.76 and 3.90mm) and length of the filter module (0.3 and 0.6m). The results of the sensitivity analysis are shown in Figure 5.

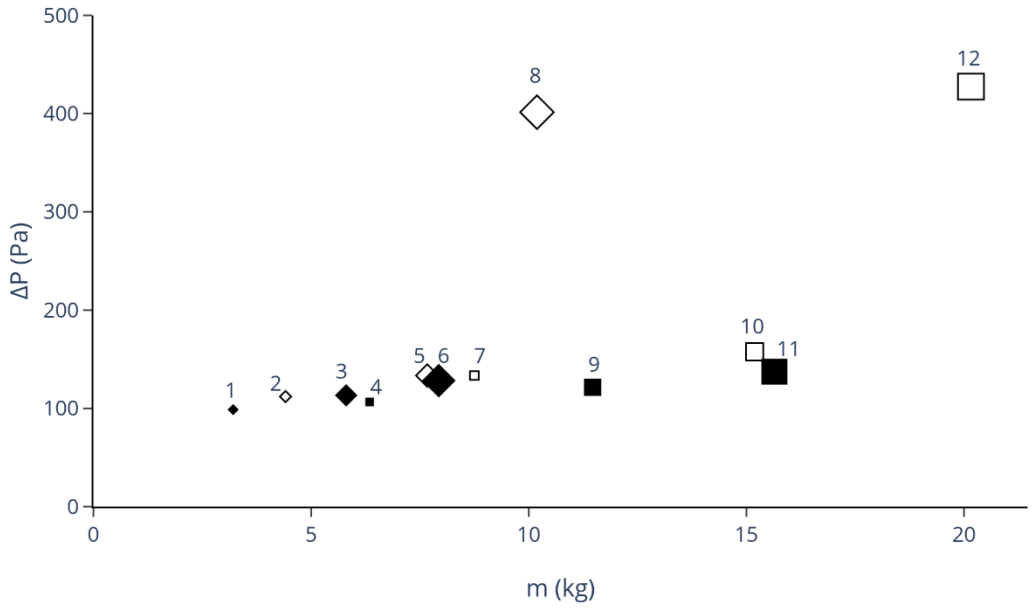

Figure 5 Visual representation of filter selection based on different filter thickness (symbol size: small =0.5mm, medium=1mm, large=1.5mm), pleat height (symbol fill: empty=2.76mm, full=3.90mm) and length (symbol type: square=0.6m; diamond 0.3m).

The most noticeable trend is that a 1.5mm filter thickness in combination with a low pleat height causes a tremendous increase in pressure drop, as in the case for configuration 8 and 12. This could be expected since the flow is first subject to high viscous stress in the small pleat channels and subsequently, it needs to permeate the thick porous layer. Both phenomena contribute to a significant energy loss. This is even better shown in Figure 6, where the pressure contours are shown for configuration 12. From this figure it is clear that viscous drag

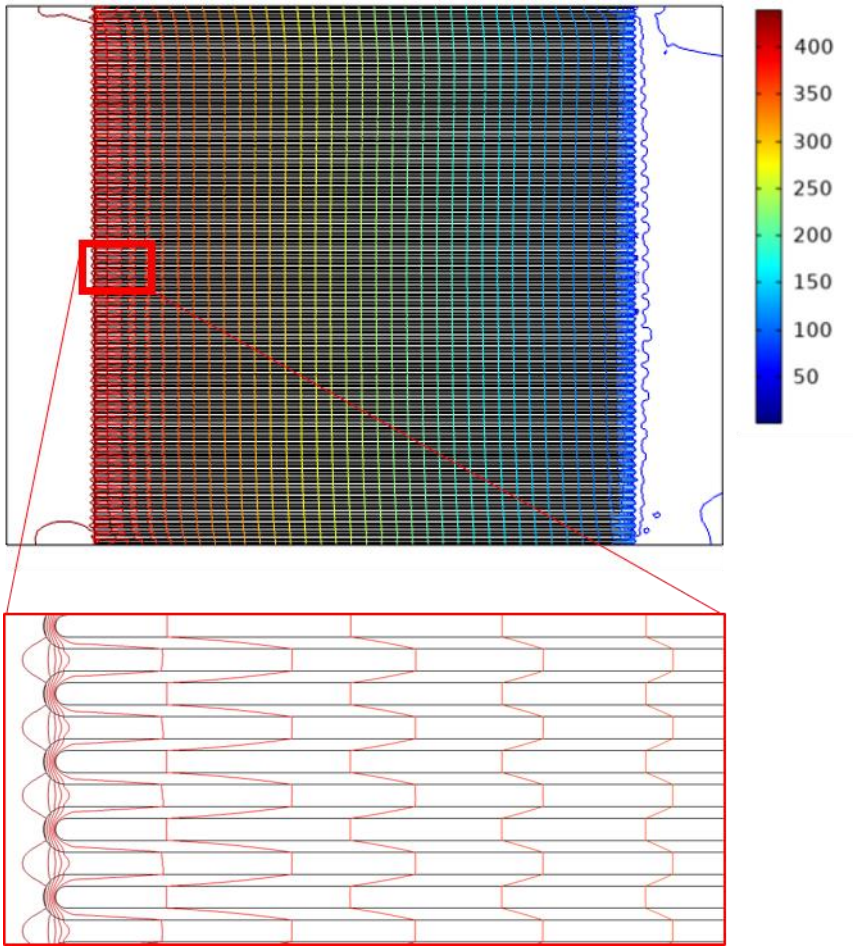

Figure 6 Pressure contours (50) of configuration 12 for an inflow velocity of 2.5 m/s

is a major contributor to the overall pressure drop, especially at the entrance region.

On the other hand, configuration 12 contains the most activated carbon of all tested setups. Remarkably, the remaining configurations all show a similar pressure drop of 100-150 Pa, while the amount of adsorbent mass is highly divergent. In general terms, it is more profitable to increase the length of the device, as this means more adsorbent mass while retaining more or less the same pressure drop. This can be explained by the fact that an increase in pressure drop is expected in elongated pleats due to more viscous drag, but also a counteracting decrease in pressure drop because of a higher filter surface area and thus a lower facial velocity. Obviously, continuously elongating the filter device is restricted by practical limitations and requires a high electrical power consumption for regeneration purposes. The same reasoning holds when analyzing the pleat height. For example, when we compare configurations 10 and 11, a similar pressure drop is observed. Configuration 10 has a pleat of height of 2.76mm, while configuration 11 has a pleat height of 3.9mm. Thus, configuration 10 is subject to higher viscous drag, but due to a thinner filter layer of 1mm, the pressure drop is very similar to setup 11 with a filter thickness of 1.5mm. Moreover, Configuration 10 contains more pleats within the same volume, but the pleats contain less activated carbon per element, resulting in a similar amount of activated carbon. The best choice of filter configuration depends on the application and customer needs. One can argue that configuration 12 is favorable because it has the highest amount of activated carbon per unit of volume. But one can also argue that configuration 11 is more favorable because it decreases the pressure drop by 67.9%, while losing only 22.4% of adsorbent mass.

4.2 Thermo-electric properties

Besides the pressure drop, the thermo-electric properties of pleated ACF filters were investigated for the 3 setups listed in Tabel 1. The goal was to derive the electrical resistivity of the ACF filter in order to estimate the filter temperature when a certain electrical power is supplied. Therefore, voltages ranging from 0 to 32V were applied to all setups and from the

amperage, the total resistance $R_{par}$was determined, according to eq. 1. Based on eq. 2 and 3, the electrical resistivity was determined and the results for all setups are shown in Figure 7. The results for Setup1 are limited to the low temperature range because R_{par} is relatively high in absence of a pleated structure, according to eq. 2. Consequently, the supplied power was limited, as well as the filter temperature. Moreover, a steep drop in electrical resistivity is observed as the filter temperature increases. Setup 2 and 3 show a very similar, slightly decreasing trend as a function of temperature. The temperature was kept under 300°C to prevent filter deterioration. Eq. 4 was fitted to the data in Figure 7 by a least square objective function , resulting in values of 0.0281 and 272.32 for ρ_0 and α_0 respectively. The resulting fit is shown in Figure 7 as well. Notice that the electrical resistivity is underestimated by eq 4. at ambient temperatures. However, regeneration temperatures below 100°C is often irrelevant, especially in the case of apolar VOCs. Figure 8 shows the required electrical power (W), derived from the applied voltage (V) and the measured current (A), to heat the ACF filter to the desired temperature, for all investigated filter setups. The x-axis is displayed in a log-scale for a better visual representation. At temperatures lower than 50°C, all setups demand equal electrical power to heat up to the same temperature. As the electrical power input increases, the surface temperature of the filter rises exponentially and therefore, a small power shift can drastically change the temperature. At higher temperatures, a divergence between the plots of setups 2 and 3 is observed. This can be explained by that fact that convective heat transfer rate differs between the setups due to a various pleat height. From a practical point of view, manually fixating the surface temperature is a difficult task and should ideally be controlled by a surface temperature sensor and a PID-controller, which can be incorporated in future prototypes.

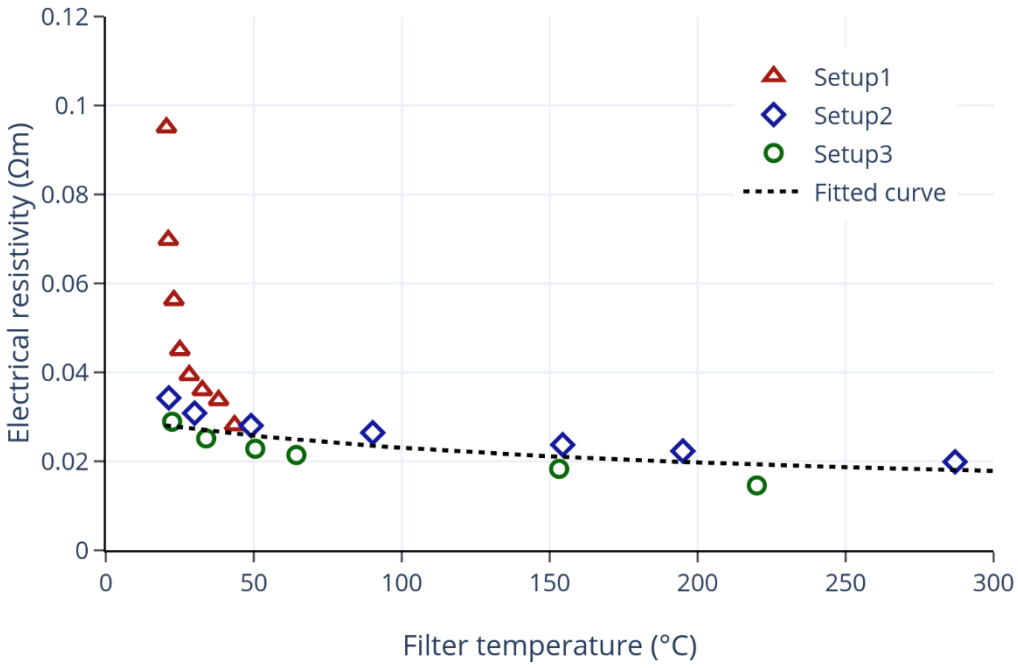

Figure 7 Electrical resistivity of the different setups in function of the filter temperature and the fitted curve according eq. 4

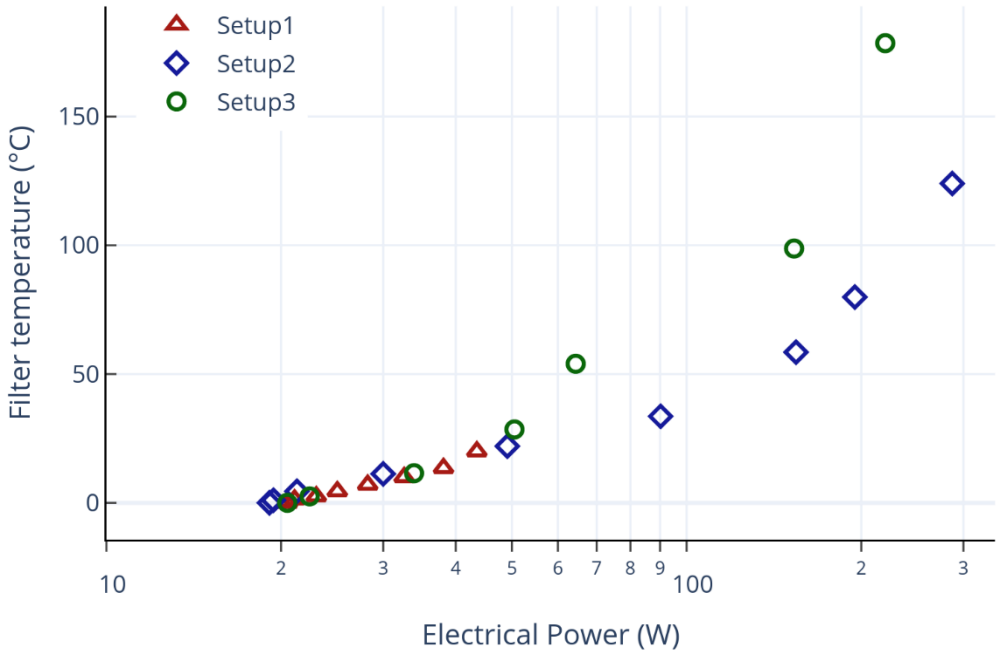

Figure 8 Filter temperature as a function of electrical power for the different setups

4.3 Adsorption/Desorption

An isotherm for acetaldehyde adsorption was constructed at 20°C, based on sequential acetaldehyde injections in a closed climate chamber with setup 2 (Figure 9). In previous work,

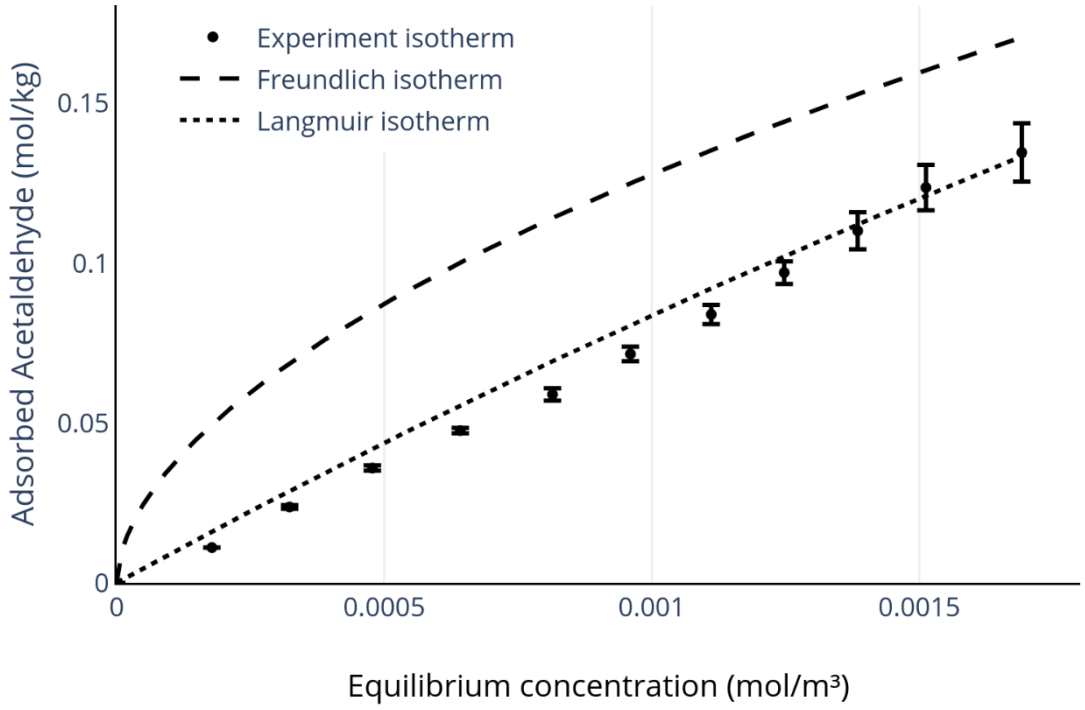

Figure 9 Acetaldehyde isotherm at 20°C and the Langmuir and Freundlich isotherms determined in previous work [8]

the adsorption curve has been described by the Freundlich isotherm, Langmuir isotherm and a linear isotherm. The latter is only applicable in small concentration ranges and since the concentration levels are an order of magnitude lower than in the previous experiments, the linear isotherm is not mentioned in this paper. Instead, the resulting adsorption isotherm is compared to the Freundlich and Langmuir relations of which the parameters are determined in previous work, i.e. $c_{ads,max}$= 0.95 mol/kg; $K_{Langm.}$=96.65 m³/mol and $1/n$=0.55; $K_{Freund.}$=5.71 (mol/kg)/(m³/mol)^n for Langmuir and Freundlich respectively.

From Figure 9 is observed that the previously determined Langmuir isotherm presents the best fit with the current adsorption data of acetaldehyde, emphasized by a R^2 of 0.978. While the Freundlich isotherm showed the best agreement with the adsorption curve in previous work, it overestimates the filters adsorption capacity at lower concentrations (R^2=0.154). The error bars on the experiment isotherm represents the standard deviation of the sequential GC-FID measurements. Based on these results, it seems reasonable to adopt the Langmuir isotherm and its respective parameters for future Multiphysics simulations. In the same way, the isotherm for toluene at 20°C was constructed and shown in Figure 10. It is clear that the ACF filters adsorption capacity is several orders of magnitude higher for toluene than for acetaldehyde. For future investigations of the ACF, it would be interesting to also include toluene adsorption in the Multiphysics model and therefore the isotherm was fitted to both Freundlich and Langmuir equation for parameterization. This resulted in $c_{ads,max}$= 1.33 mol/kg; $K_{Langm.}$=29446.59 m³/mol and $1/n$=0.38; $K_{Freund.}$=32.03 for the Langmuir (R^2=0.993) and Freundlich (R^2=0.988) equations respectively, based on a global least squares optimization function. The filters affinity for apolar compounds over polar compounds is reflected in both $c_{ads,max}$ and $K_{Langm.}$. It is not a surprise that the $c_{ads,max}$-values differ between polar and apolar compounds since they do not compete for the same adsorption sites

entirely [27]. The adsorption capacity for polar compounds is highly influenced by the surface functional groups, mostly basic and acidic groups, which are reflected by the nitrogen and oxygen content respectively. Carter et al. (2011) have shown that the adsorption of formaldehyde, a similar VOC to acetaldehyde, on the FM10 ACF cloth in particular is rather low, due to a low number of basic and acidic functional groups. The high adsorption capacity for apolar compounds is mostly reflected by the large $K_{Langm.}$-value, which indicates that the equilibrium between bulk species and adsorbed species is highly in favor of the latter, even at low concentrations.

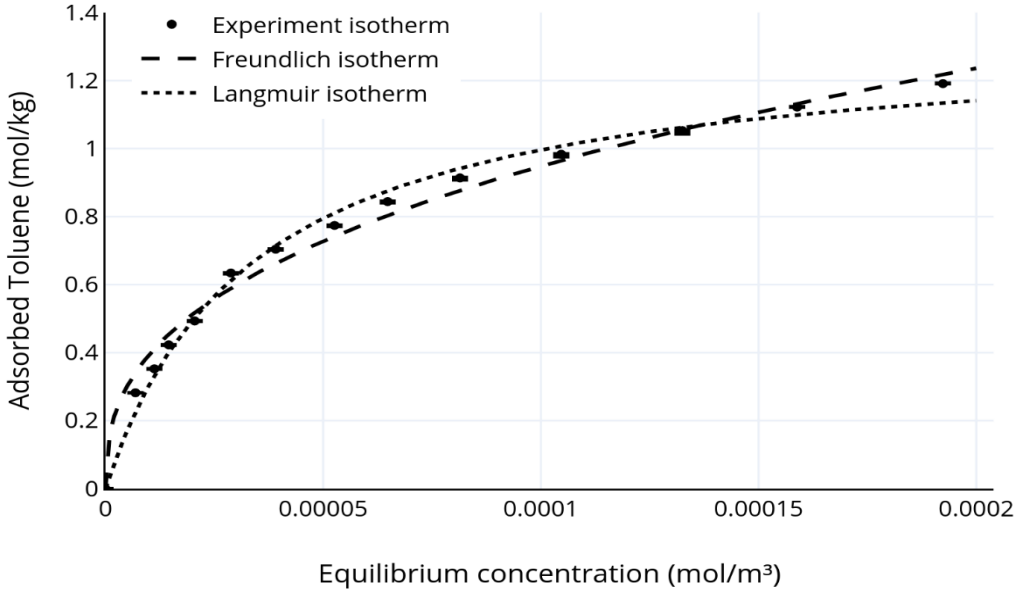

Figure 10 Toluene isotherm at 25°C and the fitted Langmuir and Freundlich isotherms

Besides the adsorption isotherm, it is interesting to establish the difference in desorption temperatures between polar and apolar compounds for regeneration purposes. The desorption efficiencies of acetaldehyde are shown in Figure 11. Notice that at a temperature of 25°C, no voltage is applied to the filter. This means that by just providing a clean air flow over the filter, more than 60% of the filters capacity can already be recuperated due to a newly established equilibrium. At 75°C surface temperature a regeneration of 98.46±0.82% was

already achieved and a temperature increase to 100°C resulted in a regeneration 99.32±1.05% filter capacity.

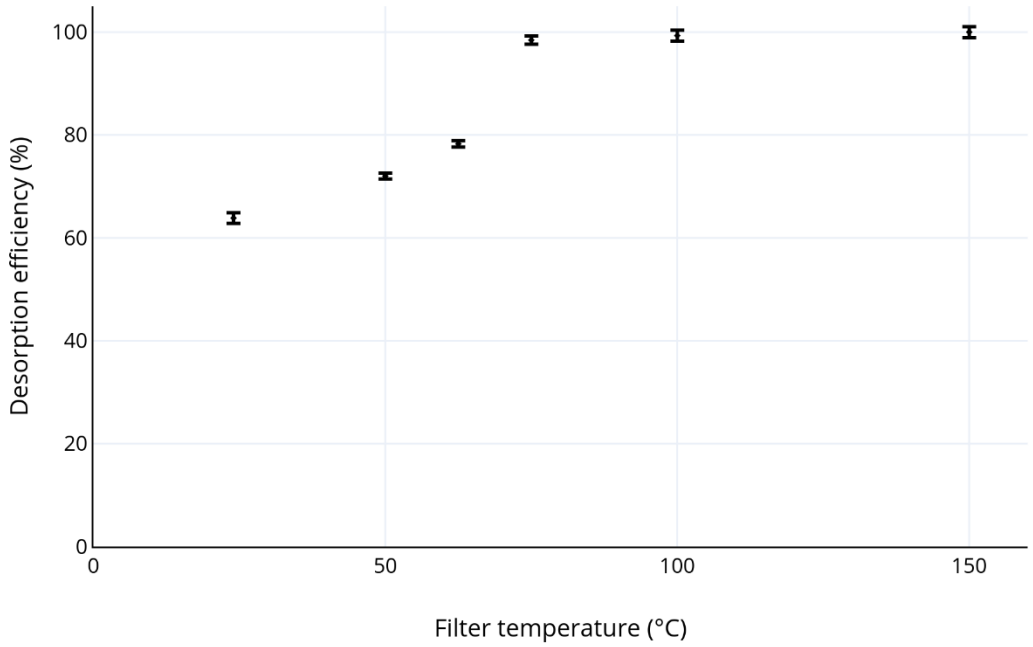

Figure 11 Desorption efficiency of acetaldehyde for different filter temperatures

The desorption efficiencies of toluene are shown in Figure 12. It is clear that desorption of toluene requires significantly higher temperatures than the weaker bound polar compound. While a large portion of acetaldehyde could be recuperated by providing a pollutant free air flow, this is definitely not the case for toluene with only 0.12±2.99% capacity regeneration. At

a surface temperature of 100°C 12.24±1.54% of the adsorbed toluene could be desorbed during a 30min period in contrast to complete regeneration of acetaldehyde at the same temperature. Total desorption of toluene was not achieved until surface temperatures above 250°C. Although at temperature of 200°C a regeneration efficiency of 98.17±1.83% was already accomplished. The comparison between desorption efficiencies at different filter temperatures of acetaldehyde and toluene emphasizes the filters affinity for apolar compounds. In reality the filter is exposed to mixtures of polar and apolar VOCs and both will be adsorbed to the filter surface. Therefore, it seems only logical to apply a minimum temperature of 200°C to ensure sufficient filter regeneration.

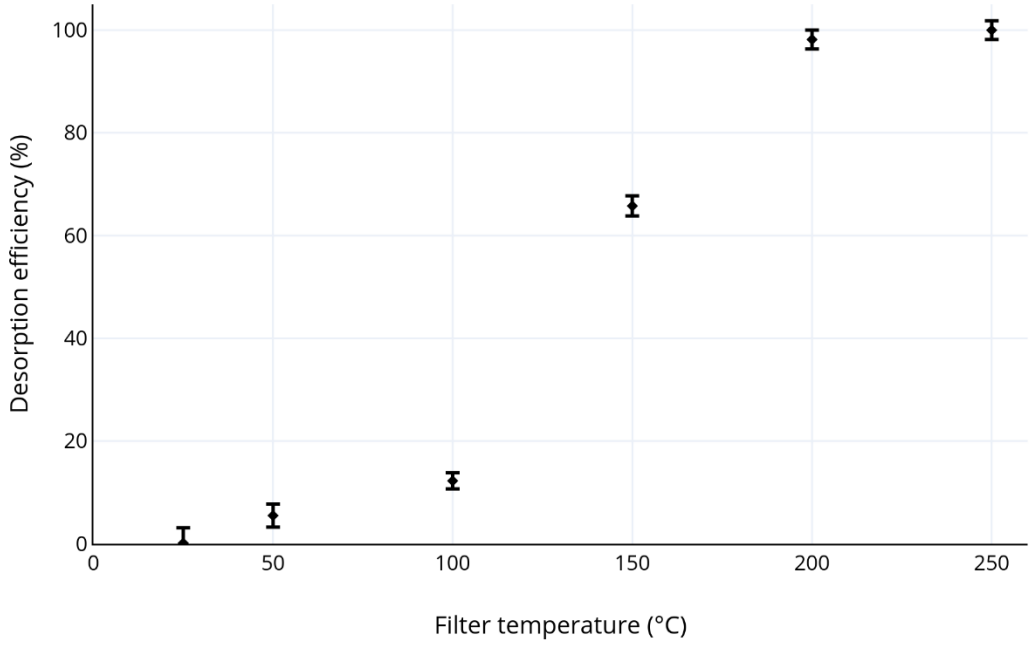

Figure 12 Desorption efficiency of toluene for different filter temperatures

5. Conclusions

This paper describes the evaluation of a novel type of activated carbon fiber filter that was developed for indoor air purification. The corrugated filter structure shows a significantly lower pressure drop when compared to a planar surface of the same filter cloth and filter thickness. The reduced pressure drop is essential to retrofit the filter into existing HVAC ducts and is therefore a major advantage of this configuration. The pressure drop at a typical HVAC flow rate was successfully validated by Computational Fluid Dynamics, using Darcy-Forchheimer parameters derived in previous work. The installation of electrodes in the tips of the filter pleats, provided a base to shape the pleated filter structure in the first place and more importantly, the capability to thermo-electrically regenerate the cloth by applying a DC voltage. We have shown that the different elements in the filter pleats behave as parallel resistances in the electrical circuit and the electrical resistivity of the filter cloth was quantified as a function of temperature. The CFD model was used to perform a virtual sensitivity study to investigate the effect of variation in pleat length, pleat height and filter thickness. Adsorption of VOCs on the ACF filter were evaluated with acetaldehyde and toluene as model compounds for polar and apolar VOCs respectively. From the results it is clear that the ACF filter tends to adsorb more apolar compounds than polar compounds and this is also reflected by the required filter temperature to desorb these compounds. Acetaldehyde could easily be desorbed, even at ambient temperature and a clean air flow. On the contrary, regeneration of a filter saturated with toluene requires temperatures higher than

200°C. This study shows the feasibility to use the ACF filter for indoor air purification and the development of a Multiphysics model that describes the fluid flow and adsorption kinetics is valuable tool to customize the filter design for different pollutant loads and flow rates.

6. Appendix

c	$Concentration\ (mol/m^3)$
c_{ads}	$Amount\ of\ adsorbed\ acetaldehyde\ (mol/kg)$
$c_{ads,max}$	$Maximum\ amount\ amount\ of\ adsorbed\ acetaldehyde\ (mol/kg)$
I	$Electrical\ current\ (A)$
$K_{Freund.}$	$Freundlich\ equilibrium\ constant\ (mol/kg)/(m^3/mol)^n$
$K_{Langm.}$	$Langmuir\ equilibrium\ constant\ (m^3/mol)$
l	$Length\ of\ a\ filter\ element\ (m)$
$1/n$	$Freundlich\ exponent\ (-)$
P	$Pressure\ (Pa)$
$R_{element}$	$Electrical\ resistance\ of\ an\ individual\ element\ of\ ACF\ (\Omega)$
R_{par}	$Parallel\ electrical\ resistance\ (\Omega)$
t	$Thickness\ of\ a\ filter\ element\ (m)$
v	$Velocity\ (m/s)$
V	$Voltage\ (V)$
w	$Width\ of\ a\ filter\ element\ (m)$
α_0	$Thermal\ coefficient\ at\ temperature\ T_0\ (K)$
β	$Forchheimer\ term\ (1/m)$
ϵ_p	$Porosity\ (-)$

κ	$Permeability\ (m^2)$
μ	$Dynamic\ viscosity\ \ (Pa \cdot s)$
μ_T	$Eddy\ viscosity\ \ (Pa \cdot s)$
ρ	$Density\ (kg/m^3)$
ρ_e	$Electrical\ resistivity\ (\Omega m)$
ρ_0	$Electrical\ resistivity\ at\ temperature\ T_0\ (\Omega m)$

7. References

[1] T.F. Cooke, Indoor Air Pollutants A Literature Review, Rev. Environ. Health. (1991). https://doi.org/10.1515/REVEH.1991.9.3.137.

[2] A. Luengas, A. Barona, C. Hort, G. Gallastegui, V. Platel, A. Elias, A review of indoor air treatment technologies, Rev. Environ. Sci. Biotechnol. (2015). https://doi.org/10.1007/s11157-015-9363-9.

[3] B. Brunekreef, S.T. Holgate, Air pollution and health, Lancet. (2002). https://doi.org/10.1016/S0140-6736(02)11274-8.

[4] J.M. Samet, M.C. Marbury, J.D. Spengler, State of Art Health Effects and Sources of Indoor Air Pollution. Part 1, AM REV RESPIR DIS. (1987).

[5] C. Jia, S. Batterman, C. Godwin, VOCs in industrial, urban and suburban neighborhoods, Part 1: Indoor and outdoor concentrations, variation, and risk drivers, Atmos. Environ. (2008). https://doi.org/10.1016/j.atmosenv.2007.11.055.

[6] R. Kostiainen, Volatile organic compounds in the indoor air of normal and sick houses, Atmos. Environ. (1995). https://doi.org/10.1016/1352-2310(94)00309-9.

[7] B. Berglund, B. Brunekreef, H. Knöppe, T. Lindvall, M. Maroni, L. Mølhave, P. Skov, Effects of Indoor Air Pollution on Human Health, Indoor Air. (1992). https://doi.org/10.1111/j.1600-0668.1992.02-21.x.

[8] J. Roegiers, S. Denys, CFD-modelling of activated carbon fibers for indoor air purification, Chem. Eng. J. 365 (2019). https://doi.org/10.1016/j.cej.2019.02.007.

[9] C. Brasquet, P. Le Cloirec, Adsorption onto activated carbon fibers: Application to water and air treatments, Carbon N. Y. 35 (1997) 1307–1313. https://doi.org/10.1016/S0008-6223(97)00079-1.

[10] A. Subrenat, J. Bellettre, P. Le Cloirec, 3-D numerical simulations of flows in a cylindrical pleated filter packed with activated carbon cloth, Chem. Eng. Sci. (2003). https://doi.org/10.1016/j.ces.2003.07.012.

[11] T. Caesar, T. Schroth, The influence of pleat geometry on the pressure drop in deep-pleated cassette filters, Filtr. Sep. (2002).

[12] L. Del Fabbro, J.C. Laborde, P. Merlin, L. Ricciardi, Air flows and pressure drop modelling for different pleated industrial filters, Filtr. Sep. (2002).

[13] D.R. Chen, D.Y.H. Pui, B.Y.H. Liu, Optimization of pleated filter designs using a finite-element numerical model, Aerosol Sci. Technol. (1995). https://doi.org/10.1080/02786829508965339.

[14] Z. Feng, Z. Long, Q. Chen, Assessment of various CFD models for predicting airflow and pressure drop through pleated filter system, Build. Environ. (2014). https://doi.org/10.1016/j.buildenv.2014.01.022.

[15] R.C. Bansal, M. Goyal, Activated carbon adsorption, 2005.

[16] M. Yao, Q. Zhang, D.W. Hand, D. Perram, R. Taylor, Adsorption and regeneration on activated carbon fiber cloth for volatile organic compounds at indoor concentration levels, J. Air Waste

Manag. Assoc. 59 (2009) 31–36. https://doi.org/10.3155/1047-3289.59.1.31.

[17] K.L. Foster, R.G. Fuerman, J. Economy, S.M. Larson, M.J. Rood, Adsorption characteristics of trace volatile organic compounds in gas streams onto activated carbon fibers, Chem. Mater. 4 (1992) 1068–1073. https://doi.org/10.1021/cm00023a026.

[18] A. Dąbrowski, P. Podkościelny, Z. Hubicki, M. Barczak, Adsorption of phenolic compounds by activated carbon - A critical review, Chemosphere. (2005). https://doi.org/10.1016/j.chemosphere.2004.09.067.

[19] X. Zhang, B. Gao, A.E. Creamer, C. Cao, Y. Li, Adsorption of VOCs onto engineered carbon materials: A review, J. Hazard. Mater. (2017). https://doi.org/10.1016/j.jhazmat.2017.05.013.

[20] F. Salvador, N. Martin-Sanchez, R. Sanchez-Hernandez, M.J. Sanchez-Montero, C. Izquierdo, Regeneration of carbonaceous adsorbents. Part I: Thermal Regeneration, Microporous Mesoporous Mater. (2015). https://doi.org/10.1016/j.micromeso.2014.02.045.

[21] D. Das, V. Gaur, N. Verma, Removal of volatile organic compound by activated carbon fiber, Carbon N. Y. 42 (2004) 2949–2962. https://doi.org/10.1016/j.carbon.2004.07.008.

[22] F. Shiraishi, T. Ishimatsu, Toluene removal from indoor air using a miniaturized photocatalytic air purifier including a preceding adsorption/desorption unit, Chem. Eng. Sci. (2009). https://doi.org/10.1016/j.ces.2009.02.024.

[23] C. Carbon, Zorflex 100% Activated Woven Carbon Cloth, (n.d.). https://d3pcsg2wjq9izr.cloudfront.net/files/3463/download/41316/47-ZorflexWovenCloth-CalgonCarbonTDS(ZORFLEX-ACC-ActivatedWovenCarbonCloth.pdf (accessed October 7, 2019).

[24] A. Subrenat, J.N. Baléo, P. Le Cloirec, Analysis of pressure drops in pleated activated carbon cloth filters, J. Environ. Eng. (2000). https://doi.org/10.1061/(ASCE)0733-9372(2000)126:6(562).

[25] J.N. Baléo, A. Subrenat, P. Le Cloirec, Numerical simulation of flows in air treatment devices using activated carbon cloths filters, Chem. Eng. Sci. (2000). https://doi.org/10.1016/S0009-2509(99)00441-8.

[26] M.A. Sidheswaran, H. Destaillats, D.P. Sullivan, S. Cohn, W.J. Fisk, Energy efficient indoor VOC air cleaning with activated carbon fiber (ACF) filters, Build. Environ. (2012). https://doi.org/10.1016/j.buildenv.2011.07.002.

[27] E.M. Carter, L.E. Katz, G.E. Speitel, D. Ramirez, Gas-phase formaldehyde adsorption isotherm studies on activated carbon: Correlations of adsorption capacity to surface functional group density, Environ. Sci. Technol. (2011). https://doi.org/10.1021/es104286d.

[28] D.B. Henschel, Cost analysis of activated carbon versus photocatalytic oxidation for removing organic compounds from indoor air, J. Air Waste Manag. Assoc. (1998). https://doi.org/10.1080/10473289.1998.10463744.

[29] Z.Z. Xie, L. Wang, G. Cheng, L. Shi, Y.B. Zhang, Adsorption properties of regenerative materials for removal of low concentration of toluene, J. Air Waste Manag. Assoc. (2016). https://doi.org/10.1080/10962247.2016.1209257.

[30] Y.K. Ryu, K.L. Kim, C.H. Lee, Adsorption and desorption of n-hexane, methyl ethyl ketone, and toluene on an activated carbon fiber from supercritical carbon dioxide, Ind. Eng. Chem. Res. (2000). https://doi.org/10.1021/ie990673u.